Functional Analysis of VopF Activity Required for Colonization in Vibrio cholerae

Functional Analysis of VopF Activity Required for Colonization in *Vibrio cholerae*

Vincent C. Tam,[a]* Masato Suzuki,[a] Margaret Coughlin,[b] David Saslowsky,[c] Kuntal Biswas,[d] Wayne I. Lencer,[c] Shah M. Faruque,[d] and John J. Mekalanos[a]

Department of Microbiology and Molecular Genetics, Harvard Medical School, Boston, Massachusetts, USA[a]; Department of Systems Biology, Harvard Medical School, Boston, Massachusetts, USA[b]; GI Cell Biology, Department of Pediatrics, Children's Hospital and Harvard Medical School, Boston, Massachusetts, USA[c]; and Molecular Genetics Laboratory, International Centre for Diarrhoeal Disease Research, Dhaka, Bangladesh[d]

* Present address: Institute for Systems Biology, Seattle, Washington, USA.

ABSTRACT ***Vibrio cholerae*, a Gram-negative facultative pathogen, is the etiologic agent for the diarrheal disease cholera. We previously characterized a clinical isolate, AM-19226, that translocates a type III secretion system (T3SS) effector protein with actin-nucleating activity, VopF, into the host cells. From comparative genomic studies, we identified a divergent T3SS island in additional isolates which possess a VopF homolog, VopN. Unlike the VopF-mediated protrusion formation, VopN localizes to stress fiber in host cells similarly to VopL, which is present in the pandemic strain of *Vibrio parahaemolyticus*. Chimera and yeast two-hybrid studies indicated that the amino-terminal regions of VopF and VopN proteins interact with distinct host cell factors. We determined that AM-19226-infected cells are arrested at S phase of the cell cycle and that VopF/VopN are antiapoptotic factors. To understand how VopF may contribute to the pathogenesis of AM-19226, we examined the effect of VopF in an *in vitro* polarized-epithelial model and an *in vivo* adult rabbit diarrheal model. Within the T3SS pathogenicity island is VopE, a homolog of YopE from *Yersinia*, which has been shown to loosen tight junctions. In polarized intestinal epithelia, VopF and VopE compromised the integrity of tight junctions by inducing cortical actin depolymerization and aberrant localization of the tight-junction protein ZO-1. An assay for pathogenicity in the adult rabbit diarrhea model suggested that these effectors are involved in eliciting the diarrheal response in infected rabbits.**

IMPORTANCE ***Vibrio cholerae* is a bacterial pathogen that causes the diarrheal disease cholera, which remains a major public health problem in many developing countries. While the major virulence factors of the pandemic *V. cholerae* strains have been characterized, new clinical strains of *V. cholerae* have arisen, causing sporadic cholera-like diseases using unknown pathogenic mechanisms. Previously, we discovered the type III secretion system in a new clinical strain of *V. cholerae* and also identified an effector protein, VopF, which is injected into the host cells and induces changes in the actin cytoskeleton. In this work, we identified a homolog of VopF that causes a distinct cellular phenotype and interactions between the effectors and host proteins. We also discovered that both effectors prevent bacterium-induced cell death in infected cells. In our tissue culture and animal models, we showed that VopF contributes to the disruption of epithelial integrity and the diarrheal response.**

Received 3 November 2010 **Accepted** 9 November 2010 **Published** 7 December 2010

Citation Tam, V. C., M. Suzuki, M. Coughlin, D. Saslowsky, K. Biswas, et al. 2010. Functional analysis of VopF activity required for colonization in *Vibrio cholerae*. mBio 1(5):e00289-10. doi:10.1128/mBio.00289-10.

Editor Jeff Miller, UCLA School of Medicine

Address correspondence to John J. Mekalanos, john_mekalanos@hms.harvard.edu.

Vibrio cholerae, a Gram-negative facultative pathogen, is the causative agent for the diarrheal disease cholera. With more than 200 serogroups, this diverse organism has been able to persist in the aquatic environment while a subpopulation has evolved to cause human disease. The O1 and O139 serogroups have caused epidemics and pandemics using toxin-coregulated pilus (TCP) and cholera toxin (CT). While non-O1, non-O139 strains have caused sporadic disease globally (1–9), the virulence mechanisms are not fully understood, since most of these strains lack TCP and CT.

Previously, we identified a type III secretion system (T3SS) in a clinical non-O1, non-O139 strain, AM-19226 (10). Furthermore, a functional T3SS was required for colonization of the small intestine in the infant mouse model (11). A type III effector, *vopF*, contains one FH1-like domain and three WH2 domains and was characterized as an actin nucleator. Delivery of VopF by infection or transfection induces actin-rich-protrusion formation in host cells (11). Recently, T3SS$^+$ non-O1, non-O139 strains have been isolated in clinical surveys and epidemiology studies of acute diarrheal diseases (12). Additionally, non-O1, non-O139 strains clearly contribute genetically to newly emerging variants of *V. cholerae*, as exemplified by a horizontal gene transfer event between non-O1 and O1 strains resulting in the evolution of epidemic O139 strains (13, 14). Therefore, it is important to monitor and understand the pathogenic mechanisms of non-O1, non-O139 strains.

From the *Vibrio* genome project, two *V. cholerae* genomes belonging to the O1 serogroup (N16961 and O395) have been completely

sequenced, and 14 additional strains have been sequenced to 5- to 8-fold coverage. We have identified a divergent T3SS island in two non-O1, non-O139 strains, 1587 and 623-39. 1587 is a clinical *V. cholerae* strain isolated from an outbreak of cholera-like illness in Lima, Peru (2); 623-39 is a diarrheal-disease clinical isolate from Dhaka, Bangladesh (S. M. Faruque, unpublished data). Within the divergent T3SS island, we have identified a *vopF* homolog, which we named *vopN*. Interestingly, VopN localizes to the host stress fibers similarly to VopL, a VopF ortholog in *Vibrio parahaemolyticus* (15). While VopF and VopN have comparable actin nucleation activities *in vitro*, we determined through the use of chimera studies that the region prior to the FH1-like domain contained the information necessary for distinct localization of the two homologous proteins. A yeast two-hybrid screen identified the distinct interacting host proteins of VopN and VopF. Furthermore, it led us to discover that both proteins have protective effects against apoptosis. Finally, using our *in vitro* and *in vivo* models, we identified that both VopE and VopF together are responsible for disrupting cell polarity and loosening tight junctions in the T84 tissue culture model as well as the diarrheal response in the removable intestinal tie-adult rabbit diarrhea (RITARD) model.

RESULTS

Identification of a divergent T3SS pathogenicity island. *Vibrio cholerae* is a diverse organism that persists in the aquatic environment. While most non-O1, non-O139 strains thrive exclusively in the environment, some have evolved pathogenic mechanisms to cause human disease independent of TCP and CT. Examination of the sequencing data of eight non-O1, non-O139 *V. cholerae* strains led to the discovery of a divergent T3SS island in strains 1587 and 623-39. The sequence homologies of the structural components between the T3SS pathogenicity islands in AM-19226 and 1587 are between 63.5% and 75.1% at the DNA sequence level (data not shown). The proteins are much more homologous (between 67 and 89.6% identity and 83.8 and 96.2% similarity) (data not shown). Due to the divergence between the nucleic acid sequences, this T3SS island was previously undetected by PCR, Southern hybridization, or genomic microarray using sequences from the AM-19226 T3SS island. Comparing the organization of the T3SS pathogenicity islands between *V. cholerae* AM-19226 and 1587 and *V. parahaemolyticus* T3SS2 (see Fig. S1 and S2 and Table S1 in the supplemental material), we have identified a central conserved region in which most of the structural components reside and two peripheral variable regions where the most diversity occurs and, coincidentally, where the putative effectors reside. The T3SS pathogenicity island identified in 1587 and 623-39 contains a divergent *vopF* homolog, which we named *vopN* (37% identity and 55% similarity at the amino acid sequence level). Amino acid sequence alignment between VopF and VopN from *V. cholerae* and VopL from *V. parahaemolyticus* (Fig. S3) indicated that VopN shares characteristics with both VopF and VopL.

VopN is an actin nucleator that localizes to the stress fibers. The VopF ortholog in *V. parahaemolyticus*, VopL, has been shown to nucleate actin *in vitro* while forming stress fibers in infected or transfected cells (15). To determine whether VopN induces protrusion formation like VopF or stress fiber formation like VopL, we transfected CHO cells with a *vopN*::*gfp* fusion construct. Actin was visualized in fixed cells by staining with Alexa Fluor 588-conjugated phalloidin, and we observed that VopN-green fluorescent protein (GFP) localized to actin stress fibers (Fig. 1A).

To gain better insight into the nature of the cellular structures that VopN and VopF induce in host cells, we conducted immunogold electron microscopy. Anti-GFP antibodies and 10-nm gold particle-conjugated antibodies were used to label VopF-GFP or VopN-GFP. *vopF*::*gfp*-transfected cells showed gold labeling enrichment along unbranched actin-rich protrusions. *vopN*::*gfp*-transfected cells, on the other hand, showed gold labeling enrichment along bundled actin cables at the cell dorsal surface (Fig. 1B). To confirm that VopN can nucleate actin *in vitro*, we determined the activity of VopN in the pyrene actin assay. Fast-performance liquid chromatography (FPLC)-purified VopN-His_6 protein has actin nucleation and polymerization activity *in vitro* similar to that of VopF (Fig. 1C).

Chimera studies for determining the domain required for inducing different cellular phenotypes. The discovery of VopF and VopN presents an interesting cell-biological question of how two homologous proteins are localized to different cellular structures. We constructed VopN/VopF hybrids in which we fused the amino-terminal half of VopF or VopN to the carboxy-terminal half of VopN or VopF, respectively. Transfection experiments with the hybrid proteins showed that VopF/N are enriched at protrusions similarly to VopF-transfected cells while the VopN/F hybrid protein localizes to stress fiber similarly to VopN-transfected cells (Fig. 2A). These results suggest that the amino-terminal halves of these type III effectors play an important role in determining protein subcellular localization. To systematically narrow down the domain or region required for stress fiber or protrusion localization, we conducted chimera studies where we fused different fragments of VopN/F to the remaining corresponding fragments of VopF/N. Transfection of these *gfp* fusion constructs led us to conclude that none of the actin-modulating domains (the FH1-like domain and three WH2 domains) contain information to differentiate the properties of the two proteins. Rather, the regions prior to the FH1-like domains are sufficient to determine the distinct cellular structure localization in host cells (Fig. 2B). To confirm that amino-terminal amino acids (aa) 1 to 84 of VopN and 1 to 135 of VopF are sufficient to differentiate the proteins from each other, we fused those fragments directly to GFP and determined their localization in transfected cells. While $VopF_{1\text{-}135}$-GFP showed uniformly distributed punctate localization across the cells, $VopN_{1\text{-}84}$-GFP localized to the actin stress fibers (Fig. 2C).

VopF and VopN interact with different host proteins. The distinct localization patterns of VopF and VopN led us to hypothesize that the two proteins interact with different host proteins. We conducted a yeast two-hybrid screen using a HeLa cell cDNA library and determined that VopN interacts with filamin A and filamin B (Fig. 3A). Filamin is a family of actin binding proteins that cross-link actin and localize to the stress fiber in tissue culture cells. Additionally, filamin acts as a scaffolding protein for signaling proteins and bridges transmembrane proteins to the actin cytoskeleton (16). Examination of the VopN truncations indicated that the portion comprising aa 1 to 84 of the VopN protein could still interact with filamin while the portion comprising aa 1 to 50 of the VopN protein could not (Fig. 3A and data not shown). These data were further corroborated by transfection and colocalization experiments with filamin (Fig. 3D). Conducting the yeast two-hybrid screen using full-length *vopF* as the bait resulted in no significant hits other than actin. As expected, full-length *vopF* and *vopN* interacted with actin while the truncated fusions that did not contain any actin-modulating domains did not. When we conducted the yeast two-hybrid screen using the truncated *vopF* gene encoding the first 135 aa (without the actin-modulating domains), we discovered interactions with the cyclophilin G (PPIG),

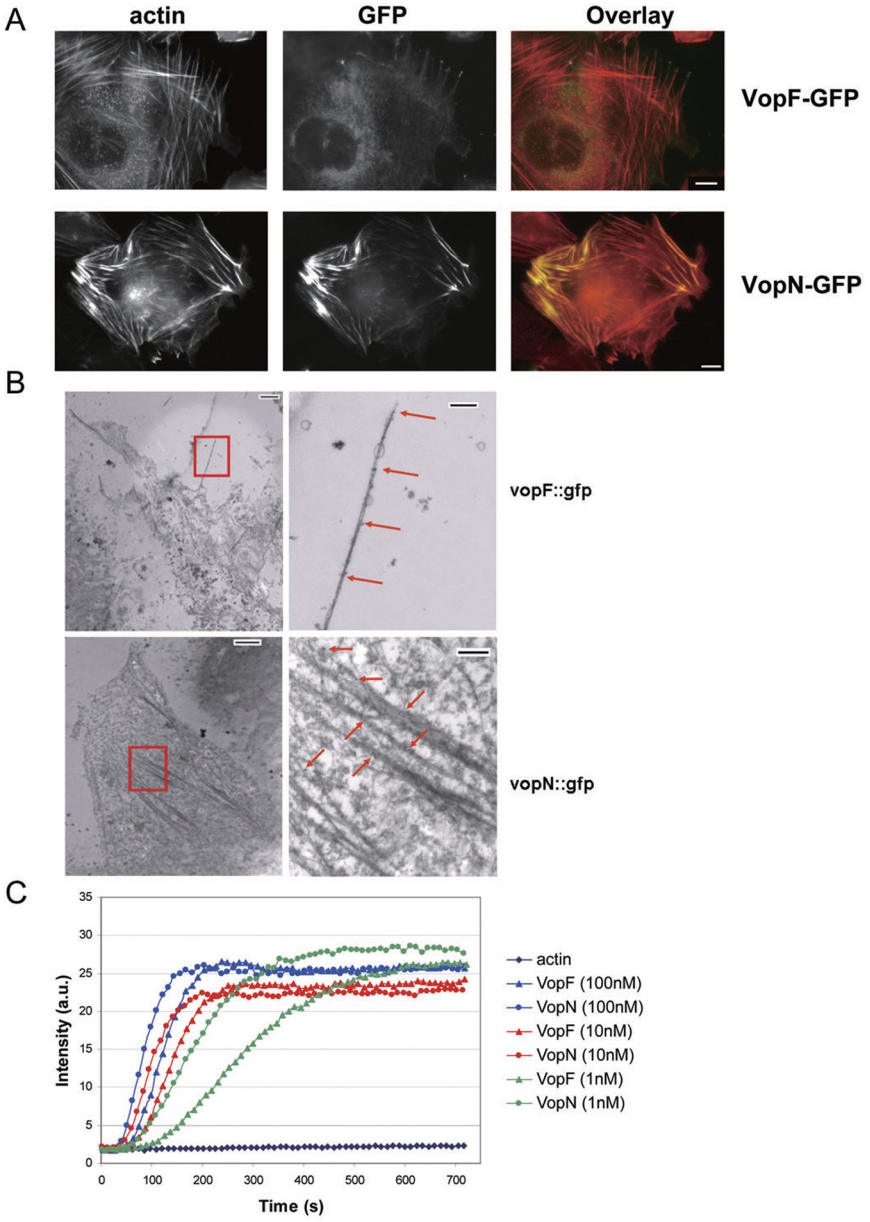

FIG 1 VopN is an actin nucleator that localizes to the actin stress fibers. (A) CHO cells were transfected with *vopF*::pAcGFP-N1 or *vopN*::pAcGFP-N1 to express VopF-GFP or VopN-GFP fusion proteins, respectively. Overlay images of Texas Red phalloidin (red) and VopF-GFP or VopN-GFP (green) are shown. Bar = 10 μm. (B) Immunogold electron micrographs of *vopF*::*gfp*- or *vopN*::*gfp*-transfected CHO cells. The two right images are higher-magnification images of the boxed areas. Red arrows point to gold labeling. Bar = 2 μm (left images) or 500 nm (right images). (C) Pyrene actin assay of VopF and VopN. VopF or VopN protein (100, 10, or 1 nM) was incubated with 2 μM monomeric pyrene-labeled actin. Actin polymerization was measured as arbitrary fluorescence intensity (in arbitrary units [a.u.]) over time (seconds), with excitation and emission wavelengths of 365 and 407 nm, respectively. A mixture of actin and pyrene actin, labeled as actin alone, served as a negative control.

breast cancer-associated gene 3 (BCA3/AKIP), and copper metabolism (Murr1) domain-containing 1 (COMMD1) proteins (Fig. 3A). Interactions between the bacterial effectors and the host proteins were confirmed using coimmunoprecipitation (Fig. 3B). PPIG is a nuclear protein that is cell cycle regulated (17). It demonstrates distinct nuclear/cytoplasmic distribution patterns during the cell cycle (17). BCA3 and COMMD1 have been shown to repress NF-κB-dependent transcription (18, 19), and COMMD1 further accelerates the ubiquitination and degradation of NF-κB subunits (20). Indeed, VopF and aa 1 to 135 of VopF, but not VopN, had the activity to inhibit tumor necrosis factor alpha (TNF-α)-induced NF-κB activation (Fig. 3C), suggesting that the binding of VopF to these nuclear proteins in the cytoplasm could exclude them from the nucleus and deregulate NF-κB activity and NF-κB-regulated normal cell functions, such as cell cycle and cell death (21, 22).

AM-19226 affects cell cycle progression *in vitro*. To investigate whether AM-19226 affects host cell responses and whether VopF plays a role in this context, we infected HeLa cells with *V. cholerae* for 4 h and then incubated the cells in medium with gentamicin for 72 h to assess the contribution of translocated effectors alone. We stained the fixed cells with propidium iodide (PI) to determine the cell cycle distribution of these cells (Fig. 4). While uninfected cells and type III mutant-infected cells have a normal cell cycle distribution, with the majority of cells in G_1 phase, cells infected with VTV18 (AM-19226Δ*endo* Δ*rtx* Δ*hly* Δ*hap*) (11) have drastically shifted from G_1 to S phase. An increase in the population of apoptotic cells (17%) was also observed in these cells. *vopF* mutant-infected cells contained an even higher proportion of apoptotic cells (31%) and almost evenly distributed populations of G_1, S, and G_2/M cells. Apoptotic cells were also visualized using terminal deoxynucleotidyltransferase-mediated dUTP-biotin nick end labeling (TUNEL) staining (see Fig. S4 in the supplemental material). The strain harboring a deletion of all actin-modulating domains of *vopF* (the VTV18 Δ*vopF* Dm2 mutant) showed a distribution similar to that of VTV18, suggesting that the actin nucleation domain of VopF is not involved in the antiapoptotic activity of the protein. Interestingly, replacing *vopF* with *vopN* resulted in a distribution similar to that of the type III mutant. These data suggest that VopF and VopN are both capable of reducing the type III-dependent apoptosis. Visualization of the infected cells suggested that the cells arrested at S phase have an enlarged nucleus and cell size indicative of cell cycle arrest. The accumulation of apoptotic cells instead of the restoration of normal cell cycle distribution that resulted from infection with the *vopF* deletion mutant suggests that there may be an unidentified cyclomodulin responsible for the cell cycle arrest.

Role of VopE and VopF in epithelial integrity and diarrheal response. As induction of cell cycle arrest by bacterial pathogens has

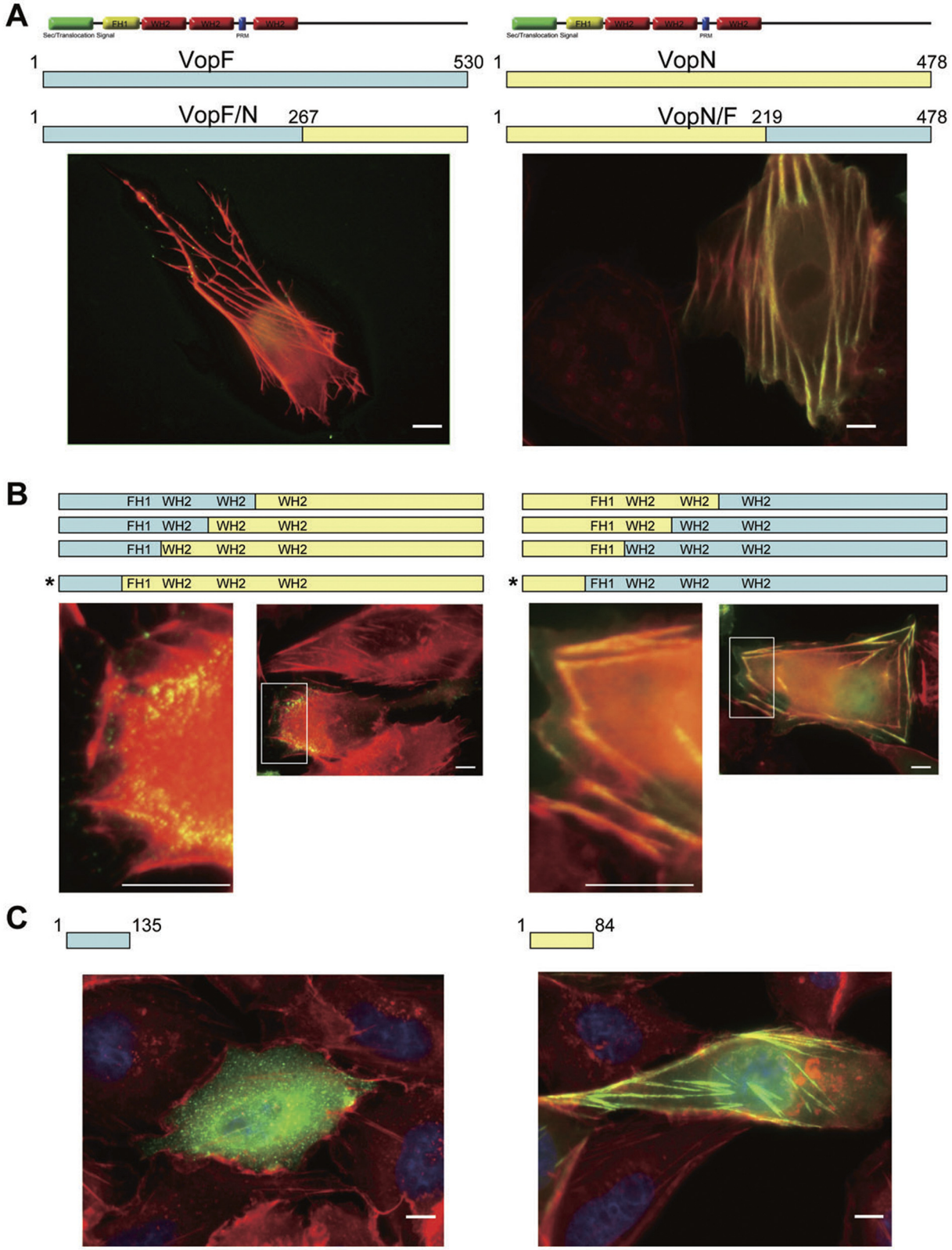

FIG 2 Domain analysis of VopF and VopN. (A) Transfection of hybrid genes comprising *vopF* and *vopN* into CHO cells. Overlay images of GFP fusion proteins (green) and actin (red) are displayed. (B) Transfection of chimera genes comprising *vopF* and *vopN* into CHO cells. Overlay images of GFP fusion proteins (green) and actin (red) are displayed. Micrographs on the left are higher-magnification images of the boxed areas. Since all four chimera genes (*vopF* and -N and *vopN* and -F) showed the same phenotype, only the bottom set of chimera genes used to generate the fluorescent micrographs is shown (asterisks). (C) Transfection of $VopF_{1\text{-}135}$-GFP and $VopN_{1\text{-}85}$-GFP into CHO cells. Overlay images of nuclei (cyan), GFP fusion proteins (green), and actin (red) are displayed. Bar = 10 μm.

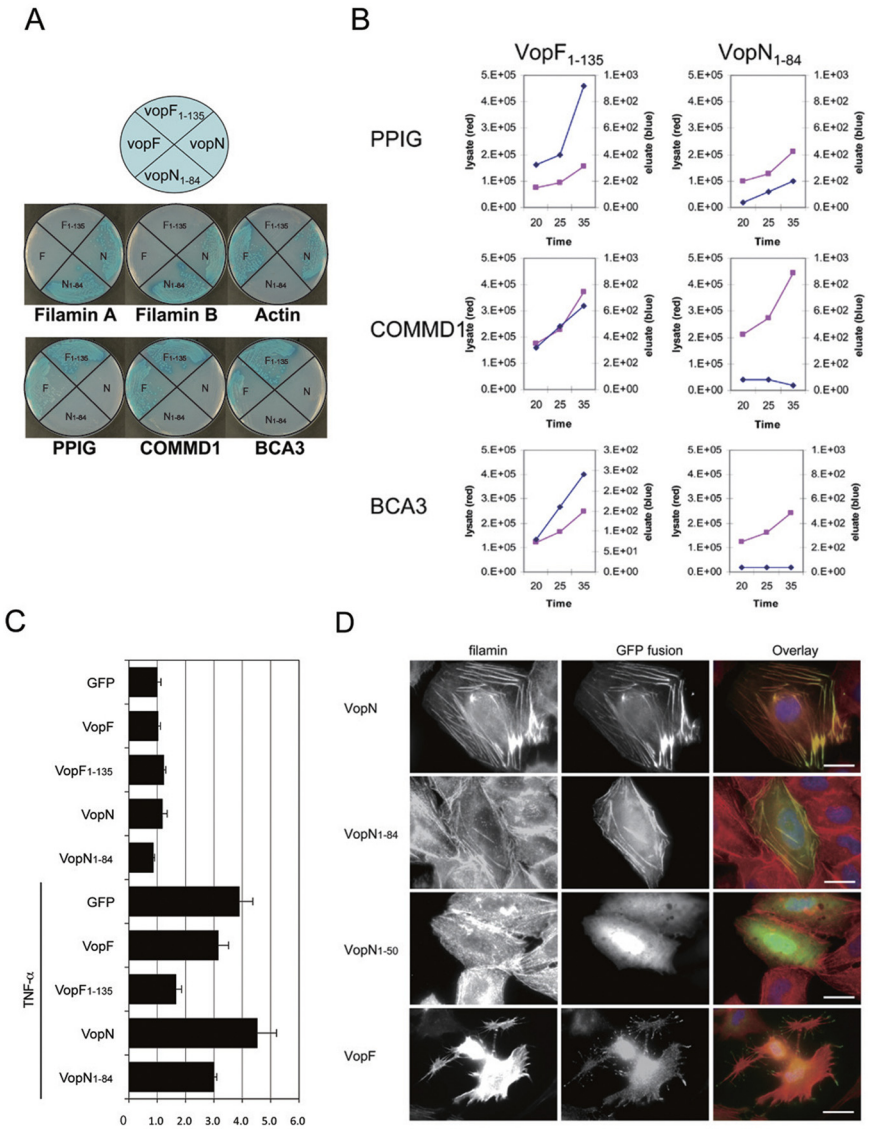

FIG 3 VopF and VopN interact with distinct host proteins. (A) A yeast two-hybrid screen identified filamin as the cellular interactor for VopN and PPIG, COMMD1, and BCA3 as the cellular interactors for VopF. The Y184 *Saccharomyces cerevisiae* host strain carrying various preys fused to the Gal4 activation domain was mated with the AH109 strain carrying full-length *vopF*, the region encoding aa 1 to 135 of *vopF*, full-length *vopN*, or the region encoding aa 1 to 84 of *vopN* fused to the Gal4 DNA binding domain. The resulting diploids were plated and restreaked onto SD–Ade–His–Leu–Trp–X-α-Gal to select for colonies strongly expressing the Ade2, His3, and Mel1 reporters. (B) Immunoprecipitation results between $VopF_{1-135}$-GFP and $VopN_{1-84}$-GFP for various preys fused to the pProLabel tag. The presence of the prey proteins was assayed by chemiluminescence in the lysates (red) and anti-GFP-immunoprecipitated fractions (blue). (C) Luciferase assays of 293T cells cotransfected with the NF-κB reporter and the indicated GFP vectors (250 ng) and stimulated with or without TNF-α (100 ng/ml). (D) Colocalization of filamin and various GFP fusion proteins. Various GFP fusion constructs were transfected into CHO cells. Filamin was stained using antifilamin antibodies. Overlay images of nuclei (cyan), GFP fusion proteins (green), and filamin (red) are displayed. Bar = 10 μm.

been hypothesized to alter epithelial integrity due to the lack of cell renewal and to prolong bacterial colonization through inhibition of cell shedding (23), we investigated the role of VopF and VopN in the context of our animal models. While we previously found that deletion of *vopF* results in a 1.5- to 2-log defect in a suckling mouse competition assay, *vopN* deletions in its native strains, 1587 and 1582 (another isolate from the same outbreak), surprisingly showed no defect in colonization when these strains competed with wild-type strains (Fig. 5A). To understand whether actin nucleation can complement a *vopF* deletion, we tested the ability of *vopN* to complement the *vopF* deletion in AM-19226. Addition of *vopN* into a *vopF*-deleted strain partially (1-log) complemented *vopF*, suggesting that while the actin nucleation activity of VopN and VopF is important, it may not be sufficient to promote efficient colonization *in vivo* (Fig. 5A). While both *vopN* and *vopF* are complemented by homologous recombination into the *vopF* locus, the level of expression and, more importantly, the translocation of VopF and VopN proteins may differ, which provides an alternate explanation for the phenotype. To understand the role of VopF and VopN in pathogenesis, they must be studied in the context of the native strains because of their unique combination of translocated effectors. Since a VopN deletion mutant of 1587 has no phenotypic defect in colonization, probably due to redundancy of the function of additional effectors, we focused on the role of VopF in its native strain, AM-19226.

Since *V. cholerae* colonizes the single-cell layer of the polarized small-intestinal epithelium, we wanted to study the interaction of AM-19226 with host cells in the more biologically relevant polarized-T84-tissue-culture-cell model. After allowing the T84 cells to differentiate in Transwell inserts for 7 days, we infected the cells with various bacterial strains and assessed the changes in transepithelial resting potential (Eo) and transepithelial resistance (TER) to determine the epithelial integrity.

In the polarized-T84-tissue-culture-cell model, a decrease of TER in the absence of increased Eo is indicative of the loosening of tight junctions. T84 cells infected with the wild-type strain VTV18 showed a 49% decrease in resistance (Fig. 5B). Cells infected with the type III structural mutant (the Δ*vcsN2* mutant) were not affected (3.4% increase), showing a level comparable to that of the medium-alone control (0.7% increase). These data suggested that the decrease in TER is type III dependent. For O1 *V. cholerae*-infected cells, a similar decrease in TER is observed, which is dependent on cholera toxin (data not shown) (24).

The T3SS island in AM-19226 carries another putative effector, which we named *vopE* because of its homology to the T3SS effector *yopE* from *Yersinia* species. VopE, like YopE, has a highly conserved GTPase-activating protein (GAP) domain. The GAP activity of YopE has been shown to inactivate RhoA, Rac1, and Cdc42 to depolymerize actin (25). VopE and VopF seem to have oppos-

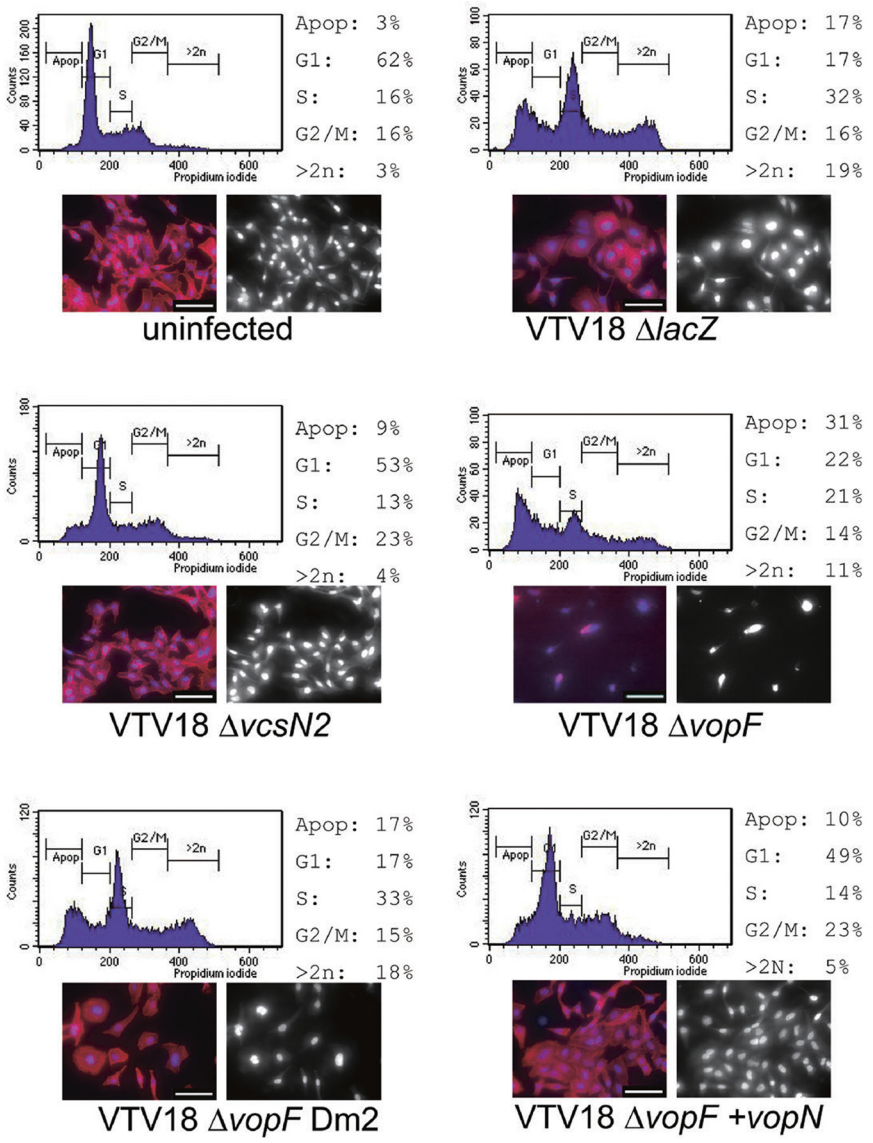

FIG 4 Cell cycle analysis. HeLa cells were infected with *V. cholerae* at an MOI of 100 for 4 h. Cells were then incubated in gentamicin for 72 h before being fixed in 75% ethanol and stained with propidium iodide. Cells were analyzed by flow cytometry. Cells were also stained for actin (red) and nuclei (cyan) for microscopy analysis. Bar = 50 μm.

ing functions, where one depolymerizes actin and the other nucleates actin. However, a pathogen possessing effectors with seemingly opposite functions has been observed previously in the *Salmonella* T3SS, where SptP is a GAP and SopE is a GTPase-exchanging factor (GEF) (26). The combination of SptP and SopE helps *Salmonella* to invade the host cells and subsequently recover the actin cytoskeleton. Deleting *vopE* has a minimal effect on colonization in the infant mouse model (data not shown). To compare the opposing functions of VopE and VopF in relation to epithelial integrity, we tested single and double mutants in the polarized-T84-cell system. Compared to the strongly decreased TER caused by VTV18, the *vopE* and *vopF* deletion mutants showed intermediate phenotypes (34.6% and 30.2%, respectively). The *vopF vopE* double mutant (24.6%) showed a more dramatic difference from VTV18. These data indicate that while *vopE* and *vopF* are involved in loosening of tight junctions, there are likely to be additional effectors involved.

To study the actin cytoskeletal organization and disruption in cell polarity in infected cells, we fixed and stained the Transwell inserts for actin, ZO-1, and AM-19226 (11) (Fig. 2C). The medium-alone control and Δ*vcsN2* mutant-infected cells showed a normal localization of ZO-1, a tight-junction protein. The *x-z* and *y-z* plane micrographs depicted that ZO-1 was localized to the apical surfaces of the polarized cells. A normal cortical actin network at the apical surface and the perijunctional actin ring was also observed. Cells infected with VTV18 showed massive depolymerization of actin, where minimal cortical actin was observed along with redistribution of ZO-1 toward the basolateral surface, consistent with loss of cell polarity and intercellular tight junctions. Δ*vopF* and Δ*vopE* mutant-infected cells also showed a certain degree of depolarization based on ZO-1 mislocalization but noticeably more-abundant cortical actin than wild-type-infected cells. In contrast, cells infected with the Δ*vopEF* mutant maintained the tight junction and cell polarity relatively well, showing somewhat normal distribution of ZO-1 and actin in large areas throughout the monolayer. Overall, these results are fully consistent with our functional measurement of epithelial barrier function as assessed by TER.

Disruption of tight-junction integrity has been identified as the common mechanism for diarrhea in gastrointestinal diseases such as ulcerative colitis (27), Crohn's disease (28), and gastritis caused by bacterial pathogens (29, 30). To correlate the results from the electrophysiology experiment with those from an *in vivo* model, we employed the removable intestinal tie-adult rabbit diarrhea (RITARD) assay to study the diarrheal response (Fig. 5D). Out of 10 animals infected with wild-type AM-19226, 9 had fatal diarrhea and 1 had nonfatal diarrhea. Δ*vcsN2* mutant-infected animals had no symptoms (10/10). The Δ*vopF* mutant, the Δ*vopE* mutant, and the double mutants all had intermediate phenotypes, ranging from fatal and nonfatal diarrhea to no symptoms. These data concur with the *in vitro* electrophysiology data indicating that *vopE* and *vopF* together strongly contribute to the disruption of tight junctions and diarrhea in infected animals.

DISCUSSION

V. cholerae is a Gram-negative bacterium that colonizes the small intestine and causes a massive diarrheal response. In the pandemic O1 and O139 strains, the toxin-coregulated pilus (TCP) is the major virulence factor that contributes to the colonization of the intestinal epithelium. After colonizing and replicating in the small intestine, the

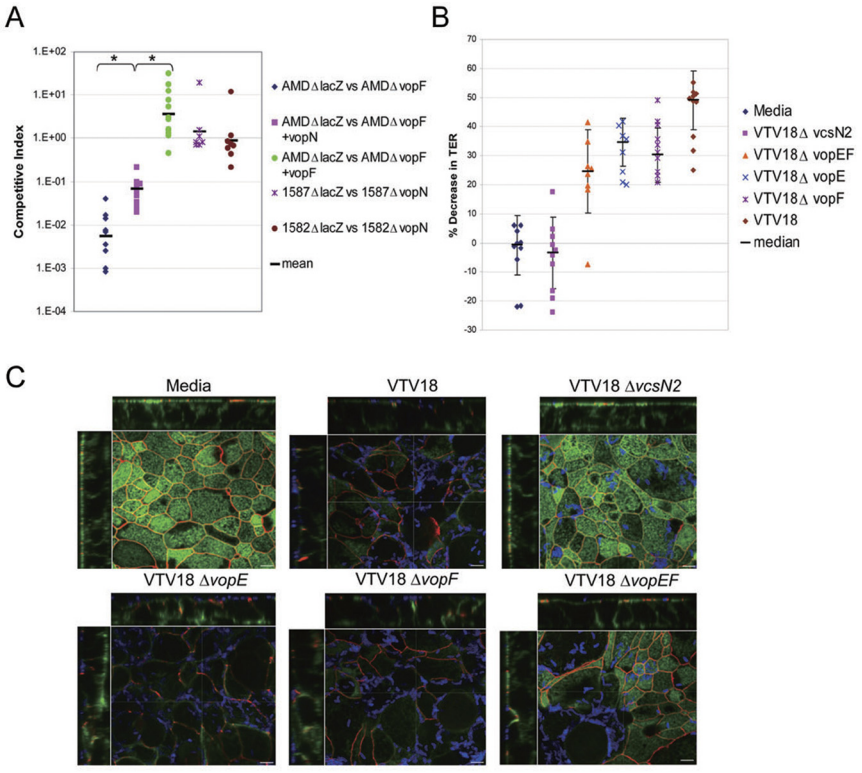

D

Strain	No. of rabbits challenged	No. responding with Fatal diarrhea[a]	Nonfatal diarrhea[b]	Fatality without diarrhea	No symptoms
AM19226	10	9	1	0	0
ΔvcsN2	10	0	0	0	10
ΔvopF	5	3	2	0	0
ΔvopE	5	2	0	0	3
ΔvopE vopF	10	5	2	1	2

[a]Rabbits developing fatal diarrhea died within 24h to 72h after initiation of diarrhea.

[b]The duration of diarrhea was between 4 and 6 days for rabbits developing non-fatal diarrhea.

The dose of bacteria used were between 5 x10^9 and 1 x 10^{10} for different strains.

FIG 5 Assay for pathogenicity in rabbits. (A) Competitive index results from the infant mouse colonization model. AMD, 1587, and 1582 show the AM-19226, 1587, and 1582 strains of *V. cholerae*, respectively. The competitive index was calculated as the ratio of the output of the test strain to the output of the reference strain over the ratio of the input of the test strain to the input of the reference strain. An asterisk denotes that the differences between the populations are statistically significant as determined by the Mann-Whitney U test ($P < 0.05$). (B) Percent decrease in TER after infection with *V. cholerae*. VTV18, a Δ*endo* Δ*rtx* Δ*hly* Δ*hap* mutant of AM-19226, was used as the wild-type strain. Values were derived by dividing the difference between the recorded resistance observed at the beginning and that observed at the end of the 180-min period by the initial resistance value. An asterisk denotes that the differences between the populations are statistically significant as determined by the Mann-Whitney U test ($P < 0.05$). (C) Confocal micrographs of T84 cells infected with *V. cholerae* strains. Overlay images of bacteria (cyan), actin (green), and ZO-1 (red) are shown. The top panel of each micrograph displays a cross section of the *x-z* plane (apical toward the top and basolateral toward the bottom), and the left panel displays a cross section of the *y-z* plane, while the main panel displays the *x-y* view onward to the apical side. (D) Diarrheal response of adult rabbits in the RITARD model.

pathogen secretes cholera toxin, which is translocated into the host cells in an AB_5 toxin-dependent manner. The O1 and O139 virulence mechanisms seem modular, requiring two separate proteins; however, the results from this study suggest that colonization and diarrheal induction are interconnected in $T3SS^+$ non-O1, non-O139 strains, with a single protein contributing to both processes.

Previously, we described a type III effector, VopF, which is an actin nucleator that induces protrusion formation in transfected or infected cells and is required for efficient colonization in the infant mouse model. In this study, we have identified a divergent T3SS pathogenicity island in additional non-O1, non-O139 strains, 1587 and 623-39, which were sequenced as part of the NIAID microbial sequencing project. This T3SS island encodes a VopF homolog, VopN. We have shown that VopN is an actin nucleator like VopF, but unlike VopF, it localizes to stress fiber, similarly to VopL from *V. parahaemolyticus*.

Chimera and transfection studies suggested that the amino-terminal portions of the proteins, preceding the FH1-like domain, are responsible for the differing localizations of the proteins in host cells. A yeast two-hybrid study identified filamin as the interacting partner for VopN. Filamin is a high-molecular-weight actin-cross-linking protein that localizes to stress fibers in cultured cells. In addition to organizing actin filaments into bundled networks, filamins may also be required for formation of filopodia. Additionally, filamin acts as a scaffolding protein for signaling proteins and bridges transmembrane proteins to the actin cytoskeleton. Interestingly, the *Salmonella* type III effectors Ssph2 and Ssel have been shown to bind filamin and inhibit actin polymerization to avoid vacuole-associated actin polymerization (31). As bacterial pathogens have evolved numerous mechanisms to manipulate the actin cytoskeleton, filamin may be a suitable target for localizing effector proteins and modulating actin dynamics. By studying the interactions of host proteins and VopF, we discovered that AM-19226 affects the cell cycle progression of infected cells and that the presence of *vopF* prevents apoptosis. While the mechanism remains to be elucidated, actin nucleation and polymerization activity of VopF are not required for the antiapoptotic activity. Numerous bacterial effectors, such as cytolethal distending toxin (CDT) and cycle-inhibiting factor (Cif) (23), have been shown to affect the eukaryotic cell cycle. Arresting the cell cycle has been proposed to benefit pathogens infecting the intestinal epithelium (23), which normally undergoes a high rate of cell turnover, with a cellular life span of less than 5 days in humans.

The newly identified VopN protein provided a tool for dissecting the actin nucleation function away from the cellular phenotype induced by the bacterial effectors. By complementing a *vopF* deletion with *vopN*, we determined that *vopN* can only partially complement the defect. Surprisingly, deletion of *vopN* in 1587 or 1582 had a min-

imal defect in colonization in the infant mouse model. The lack of a defect in colonization may be explained by the presence of a gene encoding a putative cytotoxic necrotizing factor (CNF). CNF belongs to a family of Rho GTPase-activating proteins, which includes dermonecrotic toxin (DNT) from *Bordetella*, SopE/SopE2 from *Salmonella*, IpgB1/2 from *Shigella*, and Map from enteropathogenic *Escherichia coli* (EPEC)/enterohemorrhagic *E. coli* (EHEC) (32, 33). CNF from *E. coli* has been shown to affect tight junctions (34) and forms filopodia and stress fibers (35). The presence of CNF may be functionally redundant to VopN or VopF even though CNF is found only in the 1587 T3SS and *V. parahaemolyticus* T3SS2 pathogenicity islands. Interestingly, CNF is also a cyclomodulin that induces multinucleation (23) and prevents apoptosis by remodeling the mitochondrial network (36). Although CNF is not present in the AM-19226 T3SS pathogenicity island, a type III effector named VopE was identified. VopE is a homolog of YopE from *Yersinia*. Similar to YopE, VopE has a putative GTPase-activating protein domain. By inactivating RhoA, Rac1, and Cdc42, YopE depolymerizes actin and inhibits phagocytosis by macrophages and other immune cells (25, 37). YopE has also been shown to depolarize the epithelial layer (38). Since *V. cholerae* colonizes the small intestine, which is lined with a single layer of polarized cells, we investigated how AM-19226 would interact with a polarized-T84-cell model. As the TER and confocal micrographs showed, AM-19226 translocates VopE and VopF to reorganize the actin cytoskeleton and depolarize the epithelium. Loosening the tight junctions has been a common strategy by which bacterial pathogens cause diarrhea in the human host. We investigated the diarrheal response to AM-19226 in the adult rabbit model and determined that the T3SS is required for causation of diarrhea; *vopE* and *vopF* both contribute to this phenotype.

With the discovery of the T3SS in *V. cholerae* and its role in the virulence of non-O1, non-O139 strains, it is astonishing to observe how this bacterium has evolved two independent pathogenic mechanisms to cause similar diseases. The presence of a homologous T3SS pathogenicity island in other non-O1, non-O139 *V. cholerae* strains and an orthologous T3SS2 island in the sequenced pandemic *V. parahaemolyticus* strain confirms that the T3SS has emerged to be a viable conserved pathogenic mechanism among *Vibrio* species. The genetic events and mechanisms in which virulent strains gain the ability to cause epidemics and pandemics have yet to be elucidated, and further investigation of T3SS-dependent cholera-like gastroenteritis will help us combat the disease caused by a rapidly evolving and diverse pathogen.

MATERIALS AND METHODS

Cell lines and bacterial strains. Chinese hamster ovary (CHO) cells (ATCC ccl-61) were cultivated in Ham's F-12K medium supplemented with 10% fetal calf serum (FCS) and L-glutamine (2 mM) adjusted to contain 1.5 g/liter sodium bicarbonate. HeLa, HEK293, and 293T cells were cultivated in Dulbecco's modified Eagle's medium (DMEM) supplemented with 10% fetal bovine serum (FBS) and L-glutamine (2 mM).

V. cholerae AM-19226, 1587, and 1582, non-O1, non-O139 strains of serogroup O39, O12 strains, and N16961, an O1 El Tor biotype, were used in this study. *E. coli* and *V. cholerae* strains were propagated in LB containing appropriate antibiotics at 37°C.

Strain construction. Deletion mutations were constructed by in-frame deletions of the entire reading frame using a technique described previously (39). *vopF* and *vopN* genes were complemented into the genome at the *vopF* locus using homologous recombination.

Protein expression and purification. *vopF* and *vopN* genes were cloned into pET28a (EMD Biosciences), which introduces an N-terminal fusion of the protein to a His_6 tag. BL21(DE3) strains carrying expression plasmids were subcultured 1:1,000 into 1 liter of 2× yeast extract-tryptone (YT) medium growing at 37°C with aeration until the optical density at 600 nm reached 0.5 and were induced using 0.8 mM IPTG (isopropyl-β-D-thiogalactopyranoside) and incubated at 18°C overnight. Cells were harvested and suspended in 500 mM NaCl, 50 mM Tris (pH 7.5), 10% glycerol, 15 mM imidazole, 2 mM β-mercaptoethanol and lysed by lysozyme and sonication. The fusion protein was purified by affinity chromatography using His-Trap HP (GE Health Systems).

Pyrene actin assay. The pyrene actin assay was described previously (40). Rabbit skeletal muscle actin was purified as described previously (41). Protein samples were dialyzed using Slide-a-lyzer (Pierce) in assay buffer for 2 h, and 100 nM of VopF or VopN protein was used in the assays unless specified.

Eukaryotic cell transfection. *vopF* and *vopN* and various chimera genes were cloned into pAcGFP-N1 (Clontech) to make transfection vectors expressing GFP fusion proteins. pAcGFP-N1, which encodes a GFP from *Aequorea coerulescens*, was also used as a positive control for transfection. Plasmid DNA was extracted using an endotoxin-free maxiprep kit (Qiagen).

CHO cells were seeded onto 18-mm glass coverslips (no. 1.5). jetPEI (polyPlus) transfection reagent was used as recommended by the manufacturer. At 24 h posttransfection, cells were fixed with 3.7% formaldehyde and permeabilized with 0.1% Triton X-100. Actin filaments were stained with Alexa Fluor 568-conjugated phalloidin (Invitrogen). The slides were then covered with coverslips and observed with a Nikon inverted fluorescence microscope.

Immunogold electron microscopy. CHO cells were seeded and transfected as described above. At 24 h posttransfection, cells were permeabilized with 0.1% Triton X-100 and fixed in 4% paraformaldehyde-0.025% gluteraldehyde. After being blocked with 1% fish gelatin, cells were stained with mouse monoclonal anti-GFP antibodies (1:50 dilution) (JL-8; Clontech) for 1 h and then incubated with a bridging rabbit anti-mouse antibody (1:65 dilution) for 30 min. Lastly, colloidal gold (10 nm)-conjugated secondary antibodies were incubated with the samples for 1 h. A secondary fixation was performed with 3% gluteraldehyde. Samples were postfixed with 1% osmium and stained with 1% aqueous uranyl acetate. After dehydration, a propylene oxide-epon araldite mixture was used to infiltrate the samples, which were mounted and sectioned. Microscopy was performed using a Tecnai G^2 Spirit BioTWIN, and images were captured with an AMT 2k charge-coupled-device (CCD) camera.

Yeast two-hybrid screen. *vopF* and *vopN* genes were cloned into pGBT9 (Clontech) and transformed into AH109 strains. The bait strains were screened against a pretransformed human HeLa matchmaker cDNA library (Clontech) on synthetic defined (SD)/−Ade/−His/−Trp/−Leu/X-α-Gal (5-bromo-4-chloro-3-indolyl alpha-D-galactopyranoside) agar plates. Blue colonies were restreaked multiple times to confirm the phenotype. Plasmids were rescued from *Saccharomyces cerevisiae* and transformed into *E. coli* KC8 cells. Purified DNA was reintroduced into yeast cells to confirm interactions.

Coimmunoprecipitation. Genes encoding the VopF/VopN-interacting proteins were cloned into the pProLabel-C vector using InFusion cloning (Clontech). HEK293 cells were cotransfected with $vopF_{1\text{-}135}$::pAcGFP or $vopN_{1\text{-}84}$::pAcGFP constructs and various prey fusion constructs. At 36 h posttransfection, cells were lysed using M-PER mammalian protein extraction reagent (Thermo Scientific) in the presence of protease inhibitors (Roche). GFP fusion proteins were immunoprecipitated using polyclonal anti-GFP antibodies (Clontech) with protein A Dynabeads (Invitrogen). ProLabel fusion protein was detected using a chemiluminescence ProLabel assay (Clontech). The fluorescence and chemiluminescence of the cell lysates and immunoprecipitated fractions were determined using an Envision3 plate reader (PerkinElmer).

Luciferase assay. Luciferase assays were performed using the dual-luciferase reporter assay system (Promega) according to the manufacturer's instructions. The levels of the firefly luciferase activities were measured and normalized to the activity of phRL-TK-derived *Renilla*

luciferase. The results are expressed as the means ± standard errors (SE) from triplicate experiments.

Cell cycle analysis and TUNEL staining. The cell cycle distribution and apoptotic population of HeLa cells were determined as previously described (42, 43). Briefly, ~5×10^8 HeLa cells were infected with *V. cholerae* strains at a multiplicity of infection (MOI) of 100 for 4 h. Cells were washed with phosphate-buffered saline (PBS) and incubated in medium with 100 μg/ml gentamicin for 72 h. Cells were then washed, trypsinized, fixed in 75% ethanol, and stained in a propidium iodide-RNase A solution (Invitrogen). Flow cytometric analysis was performed with a FACSCalibur flow cytometer (Becton Dickinson) using the PI emission (630 nm) for DNA quantification. Data from $>10^4$ cells were collected and analyzed using CELLQUEST software (Becton Dickinson). Apoptotic cells were stained using an APO-BrdU TUNEL assay kit (Invitrogen).

Polarized-T84-epithelial-cell infection. Electrophysiology experiments were carried out as previously described (24). Briefly, T84 cells were cultured in 0.33-cm^2 Transwell inserts in T84 medium. Experiments were performed 10 to 12 days after the plating. Cells were rinsed in Hanks' balanced salt solution and were transferred into CO_2-independent medium with 1% serum. Transwell inserts were kept at 37°C without CO_2 on a plate warmer or in an incubator for the course of the experiments. Isc and TER were measured at 10-min intervals using a dual voltage clamp device. *V. cholerae* strains were subcultured to log phase in LB at 37°C, washed, and diluted to 10^9 CFU per ml. In all experiments, 10 μl of bacteria was pipetted into the apical chamber of the Transwell insert. After the electrophysiology experiment, cells were fixed using 3.7% formaldehyde and permeabilized using 0.1% Triton X-100. Rabbit anti-AM-19226 antibodies, mouse anti-ZO-1 antibodies (Zymogen), and Alexa Fluor 568-conjugated goat anti-rabbit antibodies (Invitrogen) were used to visualize the bacteria or VopF protein. Alexa Fluor 633-conjugated phalloidin (Invitrogen) was used to stain the actin. The slides were then covered with coverslips and observed on a Nikon spinning-disk confocal microscope.

Infant mouse colonization. The infant mouse colonization assay was described previously (44). *V. cholerae* bacteria (1×10^6) were inoculated intragastrically into 5-day-old CD-1 mice (Charles River Laboratories). Infected pups were killed after 20 h, and intestinal colonized bacteria were quantified as described previously (44). A competition assay was performed by coinoculation with the Δ*lacZ* wild-type AM-19226, 1587, or 1582 strain. Differentiation of wild-type or mutant strains was based on blue/white colonies on LB plates containing X-Gal (5-bromo-4-chloro-3-indolyl-β-D-galactopyranoside). The competitive index was calculated as the ratio of the number of CFU of the test strain to the number of CFU of the reference strain divided by the ratio of the size of the inoculum of the test strain to the size of the inoculum of the reference strain. If no CFU were recovered from the intestine, a colony value of 1 was assigned to the lowest dilution.

Rabbit diarrheal assay. Diarrheal response of rabbits to *V. cholerae* was assayed by the removable intestinal tie-adult rabbit diarrhea (RITARD) model, using adult New Zealand White rabbits weighing 1.5 to 2.7 kg (45). After inoculation, rabbits were observed at 6-h intervals for 7 days for death, diarrheal severity, and shedding of challenge organisms. All rabbits that died were subjected to postmortem examination to assess the amount of fluid in the intestine.

Ethics statement. The animal experiments were performed with protocols approved by the Harvard Medical School Office for Research Protection Standing Committee on Animals. This committee approved the animal protocol used in this study. The Harvard Medical School animal management program is accredited by the Association for the Assessment and Accreditation of Laboratory Animal Care, International (AAALAC), and meets National Institutes of Health standards as set forth in the *Guide for the Care and Use of Laboratory Animals* (DHHS [NIH] publication no. 85-23, revised 1996). The institution also accepts as mandatory the PHS Policy on Humane Care and Use of Laboratory Animals by Awardee Institutions and NIH Principles for the Utilization and Care of Vertebrate Animals Used in Testing, Research, and Training. There is on file with the Office of Laboratory Animal Welfare (OLAW) an approved Assurance of Compliance (A3431-01).

Sequence and comparative genomic analysis. The BLAST-Extend-Repraze (BER) algorithm and BLAST searches were used to compare nucleic acid and amino acid sequence homologies (46, 47). Artemis version 8 from the Sanger Institute was used to visualize and annotate sequence data (48). ACT from the Sanger Institute was used to visualize BLASTn and tBLASTx comparisons (49).

Statistical analysis. The paired differences of experimental groups were compared using the nonparametric Mann-Whitney U test. A *P* value of <0.05 was considered statistically significant.

ACKNOWLEDGMENTS

We thank Fumihiko Nakamura for the antifilamin antibodies, Hao Yuan Kueh, William Brieher, and Andres Lebensohn for their helpful discussion and assistance in the pyrene actin assay, David Gondek for assistance with flow cytometry, Jessica Wagner and the Imaging and Cell Biology Cores of the Harvard Digestive Diseases Center for their assistance with confocal microscopy and analysis, and Emily Pierson for critical reading of the manuscript.

The ICDDR,B is supported by countries and agencies which share its concern for the health problems of developing countries. This work was supported by grants AI-018045 and GM-068851 from the National Institutes of Health. V.C.T. was supported by a National Science Foundation predoctoral fellowship.

SUPPLEMENTAL MATERIAL

Supplemental material for this article may be found at http://mbio.asm.org/lookup/suppl/doi:10.1128/mBio.00289-10/-/DCSupplemental.

Table S1, PDF file, 0.728 MB.
Figure S1, PDF file, 0.332 MB.
Figure S2, PDF file, 0.339 MB.
Figure S3, PDF file, 0.534 MB.
Figure S4, PDF file, 0.333 MB.

REFERENCES

1. **Bagchi, K., P. Echeverria, J. D. Arthur, O. Sethabutr, O. Serichantalergs, and C. W. Hoge.** 1993. Epidemic of diarrhea caused by *Vibrio cholerae* non-O1 that produced heat-stable toxin among Khmers in a camp in Thailand. J. Clin. Microbiol. **31**:1315–1317.
2. **Dalsgaard, A., M. J. Albert, D. N. Taylor, T. Shimada, R. Meza, O. Serichantalergs, and P. Echeverria.** 1995. Characterization of *Vibrio cholerae* non-O1 serogroups obtained from an outbreak of diarrhea in Lima, Peru. J. Clin. Microbiol. **33**:2715–2722.
3. **Dalsgaard, A., A. Forslund, L. Bodhidatta, O. Serichantalergs, C. Pitarangsi, L. Pang, T. Shimada, and P. Echeverria.** 1999. A high proportion of *Vibrio cholerae* strains isolated from children with diarrhoea in Bangkok, Thailand are multiple antibiotic resistant and belong to heterogenous non-O1, non-O139 O-serotypes. Epidemiol. Infect. **122**:217–226.
4. **Dalsgaard, A., O. Serichantalergs, A. Forslund, W. Lin, J. Mekalanos, E. Mintz, T. Shimada, and J. G. Wells.** 2001. Clinical and environmental isolates of *Vibrio cholerae* serogroup O141 carry the CTX phage and the genes encoding the toxin-coregulated pili. J. Clin. Microbiol. **39**: 4086–4092.
5. **Kamble, T. K., S. R. More, S. S. Chavan, N. D. Kulkarni, N. S. Lodha, and A. S. Kamble.** 2000. Clinical profile of non-O1 strain-O139 of *Vibrio cholerae* in the region of Ambajogai, Maharashtra. J. Assoc. Physicians India **48**:505–506.
6. **Mukhopadhyay, A. K., P. K. Saha, S. Garg, S. K. Bhattacharya, T. Shimada, T. Takeda, Y. Takeda, and G. B. Nair.** 1995. Distribution and virulence of *Vibrio cholerae* belonging to serogroups other than O1 and O139: a nationwide survey. Epidemiol. Infect. **114**:65–70.
7. **Ramamurthy, T., P. K. Bag, A. Pal, S. K. Bhattacharya, M. K. Bhattacharya, T. Shimada, T. Takeda, T. Karasawa, H. Kurazono, Y. Takeda, and G. B. Nair.** 1993. Virulence patterns of *Vibrio cholerae* non-O1 strains isolated from hospitalised patients with acute diarrhoea in Calcutta, India. J. Med. Microbiol. **39**:310–317.
8. **Rudra, S., R. Mahajan, M. Mathur, K. Kathuria, and V. Talwar.** 1996.

Cluster of cases of clinical cholera due to *Vibrio cholerae* 010 in east Delhi. Indian J. Med. Res. **103**:71–73.
9. **Sharma, C., M. Thungapathra, A. Ghosh, A. K. Mukhopadhyay, A. Basu, R. Mitra, I. Basu, S. K. Bhattacharya, T. Shimada, T. Ramamurthy, T. Takeda, S. Yamasaki, Y. Takeda, and G. B. Nair.** 1998. Molecular analysis of non-O1, non-O139 *Vibrio cholerae* associated with an unusual upsurge in the incidence of cholera-like disease in Calcutta, India. J. Clin. Microbiol. **36**:756–763.
10. **Dziejman, M., D. Serruto, V. C. Tam, D. Sturtevant, P. Diraphat, S. M. Faruque, M. H. Rahman, J. F. Heidelberg, J. Decker, L. Li, K. T. Montgomery, G. Grills, R. Kucherlapati, and J. J. Mekalanos.** 2005. Genomic characterization of non-O1, non-O139 *Vibrio cholerae* reveals genes for a type III secretion system. Proc. Natl. Acad. Sci. U. S. A. **102**:3465–3470.
11. **Tam, V. C., D. Serruto, M. Dziejman, W. Brieher, and J. J. Mekalanos.** 2007. A type III secretion system in *Vibrio cholerae* translocates a formin/spire hybrid-like actin nucleator to promote intestinal colonization. Cell Host Microbe **1**:95–107.
12. **Chatterjee, S., K. Ghosh, A. Raychoudhuri, G. Chowdhury, M. K. Bhattacharya, A. K. Mukhopadhyay, T. Ramamurthy, S. K. Bhattacharya, K. E. Klose, and R. K. Nandy.** 2009. Incidence, virulence factors, and clonality among clinical strains of non-O1, non-O139 *Vibrio cholerae* isolates from hospitalized diarrheal patients in Kolkata, India. J. Clin. Microbiol. **47**:1087–1095.
13. **Bik, E. M., A. E. Bunschoten, R. D. Gouw, and F. R. Mooi.** 1995. Genesis of the novel epidemic *Vibrio cholerae* O139 strain: evidence for horizontal transfer of genes involved in polysaccharide synthesis. EMBO J. **14**:209–216.
14. **Karaolis, D. K., R. Lan, and P. R. Reeves.** 1995. The sixth and seventh cholera pandemics are due to independent clones separately derived from environmental, nontoxigenic, non-O1 *Vibrio cholerae*. J. Bacteriol. **177**: 3191–3198.
15. **Liverman, A. D., H. C. Cheng, J. E. Trosky, D. W. Leung, M. L. Yarbrough, D. L. Burdette, M. K. Rosen, and K. Orth.** 2007. Arp2/3-independent assembly of actin by Vibrio type III effector VopL. Proc. Natl. Acad. Sci. U. S. A. **104**:17117–17122.
16. **Stossel, T. P., J. Condeelis, L. Cooley, J. H. Hartwig, A. Noegel, M. Schleicher, and S. S. Shapiro.** 2001. Filamins as integrators of cell mechanics and signalling. Nat. Rev. Mol. Cell Biol. **2**:138–145.
17. **Dubourg, B., T. Kamphausen, M. Weiwad, G. Jahreis, J. Feunteun, G. Fischer, and N. Modjtahedi.** 2004. The human nuclear SRcyp is a cell cycle-regulated cyclophilin. J. Biol. Chem. **279**:22322–22330.
18. **Ganesh, L., E. Burstein, A. Guha-Niyogi, M. K. Louder, J. R. Mascola, L. W. Klomp, C. Wijmenga, C. S. Duckett, and G. J. Nabel.** 2003. The gene product Murr1 restricts HIV-1 replication in resting $CD4^+$ lymphocytes. Nature **426**:853–857.
19. **Gao, F., J. Cheng, T. Shi, and E. T. Yeh.** 2006. Neddylation of a breast cancer-associated protein recruits a class III histone deacetylase that represses NFkappaB-dependent transcription. Nat. Cell Biol. **8**:1171–1177.
20. **Maine, G. N., X. Mao, C. M. Komarck, and E. Burstein.** 2007. COMMD1 promotes the ubiquitination of NF-kappaB subunits through a cullin-containing ubiquitin ligase. EMBO J. **26**:436–447.
21. **Hinz, M., D. Krappmann, A. Eichten, A. Heder, C. Scheidereit, and M. Strauss.** 1999. NF-kappaB function in growth control: regulation of cyclin D1 expression and G0/G1-to-S-phase transition. Mol. Cell. Biol. **19**:2690–2698.
22. **Mistry, P., K. Deacon, S. Mistry, J. Blank, and R. Patel.** 2004. NF-kappaB promotes survival during mitotic cell cycle arrest. J. Biol. Chem. **279**:1482–1490.
23. **Nougayrede, J. P., F. Taieb, J. De Rycke, and E. Oswald.** 2005. Cyclomodulins: bacterial effectors that modulate the eukaryotic cell cycle. Trends Microbiol. **13**:103–110.
24. **Fullner, K. J., W. I. Lencer, and J. J. Mekalanos.** 2001. *Vibrio cholerae*-induced cellular responses of polarized T84 intestinal epithelial cells are dependent on production of cholera toxin and the RTX toxin. Infect. Immun. **69**:6310–6317.
25. **Black, D. S., and J. B. Bliska.** 2000. The RhoGAP activity of the *Yersinia pseudotuberculosis* cytotoxin YopE is required for antiphagocytic function and virulence. Mol. Microbiol. **37**:515–527.
26. **Zhou, D., and J. Galan.** 2001. Salmonella entry into host cells: the work in concert of type III secreted effector proteins. Microbes Infect. **3**:1293–1298.
27. **Gitter, A. H., F. Wullstein, M. Fromm, and J. D. Schulzke.** 2001. Epithelial barrier defects in ulcerative colitis: characterization and quantification by electrophysiological imaging. Gastroenterology **121**: 1320–1328.
28. **Zeissig, S., N. Burgel, D. Gunzel, J. Richter, J. Mankertz, U. Wahnschaffe, A. J. Kroesen, M. Zeitz, M. Fromm, and J. D. Schulzke.** 2007. Changes in expression and distribution of claudin 2, 5 and 8 lead to discontinuous tight junctions and barrier dysfunction in active Crohn's disease. Gut **56**:61–72.
29. **Guttman, J. A., Y. Li, M. E. Wickham, W. Deng, A. W. Vogl, and B. B. Finlay.** 2006. Attaching and effacing pathogen-induced tight junction disruption in vivo. Cell. Microbiol. **8**:634–645.
30. **Pothoulakis, C.** 2000. Effects of *Clostridium difficile* toxins on epithelial cell barrier. Ann. N. Y. Acad. Sci. **915**:347–356.
31. **Miao, E. A., M. Brittnacher, A. Haraga, R. L. Jeng, M. D. Welch, and S. I. Miller.** 2003. Salmonella effectors translocated across the vacuolar membrane interact with the actin cytoskeleton. Mol. Microbiol. **48**: 401–415.
32. **Alto, N. M., F. Shao, C. S. Lazar, R. L. Brost, G. Chua, S. Mattoo, S. A. McMahon, P. Ghosh, T. R. Hughes, C. Boone, and J. E. Dixon.** 2006. Identification of a bacterial type III effector family with G protein mimicry functions. Cell **124**:133–145.
33. **Lemonnier, M., L. Landraud, and E. Lemichez.** 2007. Rho GTPase-activating bacterial toxins: from bacterial virulence regulation to eukaryotic cell biology. FEMS Microbiol. Rev. **31**:515–534.
34. **Hopkins, A. M., S. V. Walsh, P. Verkade, P. Boquet, and A. Nusrat.** 2003. Constitutive activation of Rho proteins by CNF-1 influences tight junction structure and epithelial barrier function. J. Cell Sci. **116**:725–742.
35. **Lerm, M., J. Selzer, A. Hoffmeyer, U. R. Rapp, K. Aktories, and G. Schmidt.** 1999. Deamidation of Cdc42 and Rac by *Escherichia coli* cytotoxic necrotizing factor 1: activation of c-Jun N-terminal kinase in HeLa cells. Infect. Immun. **67**:496–503.
36. **Miraglia, A. G., S. Travaglione, S. Meschini, L. Falzano, P. Matarrese, M. G. Quaranta, M. Viora, C. Fiorentini, and A. Fabbri.** 2007. Cytotoxic necrotizing factor 1 prevents apoptosis via the Akt/IkappaB kinase pathway: role of nuclear factor-kappaB and Bcl-2. Mol. Biol. Cell **18**: 2735–2744.
37. **Cornelis, G. R.** 2000. Molecular and cell biology aspects of plague. Proc. Natl. Acad. Sci. U. S. A. **97**:8778–8783.
38. **Tafazoli, F., A. Holmstrom, A. Forsberg, and K. E. Magnusson.** 2000. Apically exposed, tight junction-associated beta1-integrins allow binding and YopE-mediated perturbation of epithelial barriers by wild-type Yersinia bacteria. Infect. Immun. **68**:5335–5343.
39. **Skorupski, K., and R. K. Taylor.** 1996. Positive selection vectors for allelic exchange. Gene **169**:47–52.
40. **Ho, H. Y., R. Rohatgi, A. M. Lebensohn, and M. W. Kirschner.** 2006. In vitro reconstitution of cdc42-mediated actin assembly using purified components. Methods Enzymol. **406**:174–190.
41. **Brieher, W. M., M. Coughlin, and T. J. Mitchison.** 2004. Fascin-mediated propulsion of *Listeria monocytogenes* independent of frequent nucleation by the Arp2/3 complex. J. Cell Biol. **165**:233–242.
42. **Marches, O., T. N. Ledger, M. Boury, M. Ohara, X. Tu, F. Goffaux, J. Mainil, I. Rosenshine, M. Sugai, J. De Rycke, and E. Oswald.** 2003. Enteropathogenic and enterohaemorrhagic *Escherichia coli* deliver a novel effector called Cif, which blocks cell cycle G2/M transition. Mol. Microbiol. **50**:1553–1567.
43. **Riccardi, C., and I. Nicoletti.** 2006. Analysis of apoptosis by propidium iodide staining and flow cytometry. Nat. Protoc. **1**:1458–1461.
44. **Gardel, C. L., and J. J. Mekalanos.** 1996. Alterations in *Vibrio cholerae* motility phenotypes correlate with changes in virulence factor expression. Infect. Immun. **64**:2246–2255.
45. **Faruque, S. M., M. Kamruzzaman, I. M. Meraj, N. Chowdhury, G. B. Nair, R. B. Sack, R. R. Colwell, and D. A. Sack.** 2003. Pathogenic potential of environmental *Vibrio cholerae* strains carrying genetic variants of the toxin-coregulated pilus pathogenicity island. Infect. Immun. **71**:1020–1025.
46. **Altschul, S. F., W. Gish, W. Miller, E. W. Myers, and D. J. Lipman.** 1990. Basic local alignment search tool. J. Mol. Biol. **215**:403–410.
47. **Smith, T. F., and M. S. Waterman.** 1981. Identification of common molecular subsequences. J. Mol. Biol. **147**:195–197.
48. **Rutherford, K., J. Parkhill, J. Crook, T. Horsnell, P. Rice, M. A. Rajandream, and B. Barrell.** 2000. Artemis: sequence visualization and annotation. Bioinformatics **16**:944–945.
49. **Carver, T. J., K. M. Rutherford, M. Berriman, M. A. Rajandream, B. G. Barrell, and J. Parkhill.** 2005. ACT: the Artemis Comparison Tool. Bioinformatics **21**:3422–3423.